Journal of Inflammation Research

Dovepress
Taylor & Francis Group

Open Access Full Text Article

ORIGINAL RESEARCH

Repeated Mesenchymal Stem Cell Delivery Attenuates UHMWPE Wear Particle-Induced Osteolysis by Paracrine-Mediated Macrophage Reprogramming

Kun Ding[1,*], Dechao Fan[2,*], Ao Dong[1], Chicheng Ma[1], Teng Zeng[3], Zhen Huang[4], Yinghao Yang[5], Keguan Song[1]

[1]The Third Department of Orthopedics, The First Affiliated Hospital of Harbin Medical University, Harbin, Heilongjiang, People's Republic of China; [2]Department of Orthopedics, The First Affiliated Hospital of Dalian Medical University, Dalian, Liaoning, People's Republic of China; [3]Department of Orthopedics, The First People's Hospital of Jingzhou, First Affiliated Hospital of Yangtze University, Jingzhou, Hubei, People's Republic of China; [4]Department of Joint Surgery, Affiliated Minzu University Hospital of Hubei Minzu University, Enshi, Hubei, People's Republic of China; [5]Department of Cardiology, The First Affiliated Hospital of Harbin Medical University, Harbin, Heilongjiang, People's Republic of China

*These authors contributed equally to this work

Correspondence: Keguan Song, The Third Department of Orthopedics, The First Affiliated Hospital of Harbin Medical University, No. 23 Youzheng Street, Harbin, Heilongjiang, 150001, People's Republic of China, Email songkeguan1965@sina.com

Purpose: Periprosthetic osteolysis (PPO) induced by ultra-high molecular weight polyethylene (UHMWPE) particles remains a major clinically challenging problem in joint arthroplasty. This study investigated whether local delivery of bone marrow mesenchymal stem cells (BMSCs) could alleviate UHMWPE-induced bone destruction by modulating macrophage polarization.

Methods: In vivo, a murine calvarial osteolysis model was established and divided into four groups: Sham, UHMWPE-induced osteolysis (PIO), single BMSC injection (BMSCs-1), and repeated BMSC injection (BMSCs-2) groups. In vitro, RAW264.7 macrophages were treated under five conditions: RAW264.7 alone, BMSCs alone, RAW264.7+BMSCs, RAW264.7 + UHMWPE, and RAW264.7 + UHMWPE + BMSCs in a transwell co-culture system. Bone parameters (BMD, BV/TV, Tb.Th, and Tb.N) were evaluated by micro-CT; Macrophage polarization and cytokine expression were assessed by histology, immunohistochemistry (IHC), flow cytometry, ELISA, and immunofluorescence.

Results: In vivo, BMSC administration markedly improved bone parameters and mitigated UHMWPE-induced osteolysis, with repeated dosing showing more efficacy than a single dose compared to the PIO group. BMSC treatment suppressed M1 (CD80+) macrophage infiltration, enhanced M2 (CD206+) polarization, and rebalanced cytokine expression by reducing TNF-α and increasing IL-10 levels. In vitro, the BMSC transwell co-culture system consistently promoted M2 polarization and anti-inflammatory cytokine secretion in UHMWPE-stimulated macrophages, confirming the paracrine-mediated immunomodulatory effect.

Conclusion: Local BMSC therapy, particularly with repeated dosing, effectively attenuated UHMWPE-induced osteolysis by reprogramming macrophage polarization through paracrine signaling. These findings highlight a potential translational strategy for stem cell-based treatment of periprosthetic osteolysis.

Keywords: osteolysis, macrophage activation, bone marrow mesenchymal stem cells, polyethylene, inflammation

Introduction

Total joint arthroplasty (TJA) is widely recognized as one of the most effective surgical interventions for managing end-stage joint disease and offers significant pain relief and functional restoration.[1,2] However, the long-term success of TJA is often compromised by aseptic loosening caused by wear particle-induced periprosthetic osteolysis (PPO), which remains the leading cause of prosthesis failure and revision surgeries worldwide.[3,4] Among the various types of wear

Received: 6 August 2025
Accepted: 27 October 2025
Published: 11 November 2025

debris generated during implant use, ultra-high molecular weight polyethylene (UHMWPE) particles are the most prevalent in modern joint prostheses because of their widespread application as bearing materials.[5,6] However, prolonged mechanical wear releases a large number of UHMWPE particles into the peri-implant microenvironment, triggering chronic inflammation and progressive bone resorption.[3,7]

Recent projections indicate that the demand for TJA will continue to increase significantly over the coming decades.[8] For example, projected models based on Medicare data anticipate a 176% increase in total hip arthroplasty (THA) and a 139% increase in total knee arthroplasty (TKA) by 2040, with further growth expected by 2060, similar trends have been reported in other predictive models.[9–11] Concurrently, the incidence of osteoporotic fractures and other bone-related conditions is rising with demographic aging, emphasizing the urgent need for preventive and regenerative strategies to preserve bone integrity and long-term implant stability.[12–14]

UHMWPE and titanium particles have been implicated in the pathogenesis of PPO, and despite differences in their physicochemical properties, they share similar macrophage-mediated inflammatory pathways.[15,16] Once released, wear particles are recognized and internalized by local immune cells, particularly macrophages, triggering a cascade of chronic inflammatory responses.[17] These immune reactions disrupt the bone remodeling balance, primarily by promoting osteoclast differentiation and activity, ultimately leading to progressive bone loss around the prosthesis.[18,19] Mounting evidence suggests that the imbalance between pro-inflammatory M1 and anti-inflammatory M2 macrophages plays a pivotal role in this pathological process.[20,21] M1 macrophages secrete tumor necrosis factor-alpha (TNF-α), interleukins (IL-1β, IL-6), and reactive oxygen species (ROS), which stimulate osteoclastogenesis.[22] In contrast, M2 macrophages support inflammation resolution and tissue regeneration through IL-10 and TGF-β secretion.[23] Therefore, Macrophage polarization has emerged as a therapeutic target to prevent or reverse periprosthetic bone loss.[24]

Various strategies have been explored to modulate this polarization, such as surface modification of implants, local delivery of anti-inflammatory agents, and use of immune-modulating biomaterials.[25] However, these approaches often lack long-term efficacy or are difficult to implement clinically.[26,27] Cell-based therapies, particularly those involving mesenchymal stem cells (MSCs), are gaining traction owing to their immunomodulatory potential and regenerative properties.

Bone marrow-derived mesenchymal stem cells (BMSCs) possess multipotent differentiation potential and exert profound immunomodulatory effects on both innate and adaptive immune systems. Through direct cell-cell contact and paracrine signaling, BMSCs can suppress M1 polarization and promote M2 macrophage differentiation.[28] By secreting a range of soluble factors, including IL-10, PGE2, TSG-6, and TGF-β, and modulating key inflammatory signaling pathways, such as the NF-κB, STAT3, and PI3K/Akt pathways.[29,30] Clinical and preclinical studies have demonstrated the efficacy of MSC-based therapy in promoting bone repair, reducing inflammation, and improving outcomes in degenerative and osteoporotic bone diseases.[31–33] In orthopedic applications, bone marrow-derived mesenchymal stem cells (BMSCs) have shown the ability to regulate the local immune microenvironment, inhibit osteoclastogenesis, and enhance osteogenesis, providing dual benefits in restoring bone balance and mitigating inflammation, which may be highly relevant in lesions involving both bone resorption and inflammation-driven bone loss.[34,35]

However, the mechanistic understanding of how BMSCs regulate macrophage polarization and cytokine production in the presence of UHMWPE wear particle-induced osteolysis remains incomplete. Although BMSCs have demonstrated promising therapeutic effects in various inflammatory diseases, their specific roles in orthopedic settings, particularly in wear particle-induced periprosthetic osteolysis, remain to be fully elucidated. In particular, the influence of BMSCs on macrophage polarization and remodeling of the local immune microenvironment has not been systematically studied. The signaling networks and cellular interactions underlying these effects remain unclear and require further investigation.

Objective: Therefore, this study aims to conduct a comprehensive evaluation of the regulatory effects of BMSCs on macrophage polarization and inflammatory cytokine secretion in response to UHMWPE particles. By integrating an in vitro co-culture system with an in vivo murine calvarial osteolysis model, we assessed the immunomodulatory mechanisms of BMSCs, the impact of treatment frequency on therapeutic efficacy, and their influence on local bone microarchitecture and cytokine profiles.

By uncovering how BMSCs reprogram macrophage phenotypes and reshape the peri-implant immune milieu, this study seeks to provide a mechanistic foundation for the development of stem cell–based precision immunotherapies or advanced biofunctionalized materials for preventing UHMWPE wear particle-induced osteolysis.

Materials and Methods

Preparation of UHMWPE Wear Particles

The UHMWPE particles (Nanochemazone, Leduc, Alberta, Canada) had a mean particle diameter of 2.6 μm (range from <0.6 to 21 μm), measured by scanning electron microscopy according to the manufacturer's specifications.[36,37] The particles were immersed in 70% ethanol for 24–48 hours, rinsed with sterile PBS, and UV-sterilized for 30 minutes. The particles tested negative for endotoxin using a Limulus Amebocyte Lysate Kit (Beyotime Biotechnology, Shanghai, China). Particles were suspended in DMEM (Gibco, NY, USA) and stored at 4 °C. To prevent aggregation, the suspension was ultrasonicated for 15–30 min before use.

Isolation and Culture of BMSCs

Bone marrow-derived mesenchymal stem cells (BMSCs) were isolated from the femurs and tibias of 2-week-old C57BL/6 mice using the compact bone explant method, as previously described.[38,39] Cells were cultured in α-Minimum Essential Medium (α-MEM; Gibco, Grand Island, NY, USA) supplemented with 10% fetal bovine serum (FBS, Gibco, Grand Island, NY, USA) and 1% penicillin-streptomycin (Gibco, Grand Island, NY, USA). Cells at passages 3–5 were used for subsequent experiments. To verify their identity and multipotency, BMSCs were induced to differentiate into osteogenic, adipogenic, and chondrogenic lineages using a standard induction medium. Differentiation was confirmed by Alizarin Red S, Oil Red O, and Alcian Blue staining (Sigma-Aldrich, St. Louis, MO, USA).

Culture of RAW264.7 Macrophages

The RAW264.7 cell line was purchased from Procell Life Science & Technology Co., Ltd. (Wuhan, China). The cells were cultured in DMEM supplemented with 10% FBS (FBS, Gibco, Grand Island, NY, USA) and 1% penicillin-streptomycin (Gibco, Grand Island, NY, USA), and maintained at 37°C in a humidified incubator with 5% CO_2. The culture medium was refreshed every 2–3 days, and cells in the logarithmic growth phase were used for experiments.

Determination of UHMWPE Particle Concentration

To determine the appropriate concentration of UHMWPE particles for macrophage polarization assays, RAW264.7 cells were treated with varying concentrations (0.05, 0.1, 0.2, and 0.8 mg/mL) for 24 hours. The expression of the M1 marker CD80 and M2 marker CD206 was assessed using flow cytometry, and the $CD80^+/CD206^+$ cell ratio was calculated to evaluate the polarization shift.

Co-Culture of BMSCs and RAW264.7 Cells Using a Transwell System

A non-contact co-culture system was established using Transwell plates with 0.4 μm pore size membrane inserts (Corning, NY, USA). RAW264.7 macrophages were seeded into the lower chambers (1×10^5 cells/well) in 1 mL DMEM with 10% FBS. For the particle-treated groups, the UHMWPE particles were added at a final concentration of 0.2 mg/mL. After 12 h, BMSCs (1×10^5 cells/well) were seeded into the upper inserts in 1 mL α-MEM with 10% FBS and co-cultured for 24 h at 37°C with 5% CO_2. Five groups were included: A. RAW264.7 alone (M), B. BMSCs alone (BMSCs), C. co-culture without particles (M + BMSCs), D. RAW264.7 with particles (M + UPE), and E. co-culture with particles (M + UPE + BMSCs). After incubation, the supernatants were collected, centrifuged, and stored at −80°C for cytokine assays. RAW264.7 cells were harvested for flow cytometry and immunofluorescence analysis.

Flow Cytometry Analysis

Flow Cytometric Characterization of BMSCs

Flow cytometry (ACEA Biosciences Inc., Hangzhou, China) was performed using a panel of surface markers.BMSCs were harvested, washed, and stained with fluorochrome-conjugated antibodies (BioLegend, San Diego, CA, USA), including CD31-FITC, CD45-FITC, CD34-PE, Sca-1-PE, CD90-APC, CD105-APC, CD11b-PerCP-Cy5.5, and CD44-PerCP-Cy5.5. Isotype controls were used to assess nonspecific binding. At least 10,000 events per sample were acquired and analyzed using FSC/SSC gating to exclude debris and doublets.

Macrophage Polarization of RAW264.7 Cells

After co-culture, RAW264.7 cells were harvested, washed, and stained with F4/80-PerCP-Cy5.5, CD80-PE, and CD206-APC (BioLegend, San Diego, CA, USA). Isotype-matched controls were used to assess nonspecific binding. At least 10,000 events were recorded for each sample, and gating strategies were used to quantify the proportions of M1 (F4/80 +CD80+) and M2 (F4/80+CD206+) macrophages.

Enzyme-Linked Immunosorbent Assay (ELISA)

The concentrations of the inflammatory cytokines TNF-α and IL-4 in the culture supernatants were quantified using ELISA kits (Cusabio, Wuhan, Hubei, China) according to the manufacturer's protocol. Absorbance was measured at 450 nm using a microplate reader (Bio-Rad, Hercules, CA, USA), and cytokine concentrations were calculated based on standard curves.

Immunofluorescence Staining

After co-culture, the cells were fixed with 4% paraformaldehyde (Solarbio, Beijing, China), permeabilized with 0.1% Triton X-100 (Solarbio, Beijing, China), and blocked in 1% bovne serum albumin (BSA, Solarbio, Beijing, China). The cells were then incubated with antibodies against F4/80 (red) and either CD80 or CD206 (green, BioLegend, San Diego, CA, USA), followed by nuclear counterstaining with DAPI (blue, Beyotime, Shanghai, China). Fluorescence images (Leica Microsystems, Wetzlar, Germany) were acquired, and merged channels were used to assess marker colocalization with F4/80-positive macrophages.

Mouse Calvarial Osteolysis Model Induced by UHMWPE Particles

C57BL/6 male mice (2–3 weeks old) were purchased from Vital River Laboratory Animal Technology Co., Ltd (Beijing, China). The protocols implemented in this study adhered to internationally recognized standards and were approved by the Animal Ethics Committee of the First Affiliated Hospital of Harbin Medical University. A murine calvarial osteolysis model was established using 4-week-old male C57BL/6 mice (n=4/group). After anesthesia with 4% chloral hydrate (Solarbio, Beijing, China), a midline incision was made to expose the parietal bone, and a UHMWPE particle suspension (0.2 mL, 10 mg/mL) or 0.2 mL PBS was applied to the calvarial surface. Mice were randomly assigned to four groups: A. Sham (PBS), B. PIO (UHMWPE), C. BMSCs-1 (UHMWPE + BMSCs on day 7), and D.BMSCs-2 (UHMWPE + BMSCs on days 7 and 14). BMSCs were subcutaneously administered at a dose of 1×10^6 cells in 0.2 mL PBS. All mice were sacrificed on day 21 for analysis.

Micro-Computed Tomography (Micro-CT) Analysis

Calvarial samples were scanned using a VNC-102 micro-CT scanner (VINNO, Suzhou, China) at 90 kV and 0.09 mA with a voxel size of 10 μm. Soft tissue and residual particles were removed before scanning. Three-dimensional reconstructions were generated, and bone parameters were evaluated within a standardized region of interest near the sagittal suture.

Histological and Immunohistochemical (IHC) Analyses

After micro-CT scanning, calvarial samples were decalcified in 10% EDTA (Solarbio, Beijing, China) for 14 days at room temperature, dehydrated, embedded in paraffin, and sectioned at 5 μm. Hematoxylin and eosin (HE) staining was performed to evaluate histological changes.

For IHC, the sections were deparaffinized, antigen retrieval was performed in citrate buffer (pH 6.0, Beyotime, Shanghai, China), and nonspecific binding was blocked with 3% BSA. The Slides were incubated overnight at 4 °C with primary antibodies against CD80 (BioLegend, San Diego, CA, USA) and CD163 (Abcam, Cambridge, UK), followed by incubation with HRP-conjugated secondary antibodies (Abcam, Cambridge, UK). DAB was used for color development, and nuclei were counterstained with hematoxylin. IHC-staining was visualized by Leica DM microscope (Leica Microsystems, Wetzlar, Germany).

ELISA for Mouse Tissue Samples

Periosteal tissue samples were collected on day 21 post-surgery, homogenized in lysis buffer containing protease inhibitors, and centrifuged. Supernatants were used to quantify TNF-α and IL-4 levels using ELISA kits (Cusabio, Wuhan, Hubei, China). Subsequent steps followed the same procedure as the ELISA assay described earlier.

Flow Cytometry of Tissue-Derived Cells

Periosteal tissues were enzymatically digested with collagenase I, hyaluronidase, and Dnase (Solarbio, Beijing, China) at 37 °C, filtered through a 40 μm mesh, and washed with PBS. Single-cell suspensions (1×10^6 cells/mL) were stained with F4/80-PerCP-Cy5.5, CD80-PE, and CD206-APC. After incubation and washing, ≥10,000 events per sample were collected and analyzed. Macrophage subsets were defined as M1 (F4/80+CD80+) and M2 (F4/80 +CD206+).

Statistical Analyses

All experiments were performed in triplicate as independent biological replicates. Data are presented as mean ± standard deviation (SD). Data normality was assessed using the Shapiro–Wilk test in GraphPad Prism 9.0 (GraphPad Software, San Diego, CA, USA). Most data sets showed no significant deviation from a normal distribution ($p > 0.05$), while a few groups exhibited slight deviations ($p < 0.05$). Given that the overall data were approximately normally distributed, parametric tests were applied for statistical comparisons. Comparisons between two groups were made using an unpaired two-tailed Student's *t*-test, and one-way ANOVA followed by Tukey's post hoc test was used for multiple group comparisons. Statistical significance was set at $P < 0.05$ (*$P < 0.05$, **$P < 0.01$, ***$P < 0.001$).

Results

Characterization of BMSCs Isolated from Mouse Bone Marrow

BMSCs were successfully isolated from mouse femurs and tibias using the compact bone adhesion method (Figure 1A). By day 3 of primary culture, fibroblast-like cells had migrated from the bone fragments and adhered to the flask surface. They proliferated rapidly and gradually formed whirlpool-like colonies, and by 10–14 days, most cells exhibited a spindle-shaped morphology, characteristic of mesenchymal stem cells (Figure 1B).

To confirm their multipotency, BMSCs were subjected to trilineage differentiation. After 14 days, Alizarin Red S staining revealed extensive calcium deposition, confirming osteogenic differentiation. Oil Red O staining identified intracellular lipid droplets indicative of adipogenic differentiation, whereas Alcian Blue staining demonstrated glycosaminoglycan-rich extracellular matrix deposition, confirming chondrogenic potential (Figure 1C).

Flow cytometry further validated the immunophenotypic profiles of the isolated cells. BMSCs showed strong expression of CD44, CD90, CD105, and Sca-1, whereas hematopoietic and endothelial markers (CD31, CD34, CD45, CD11b) were almost absent compared to the isotype controls, meeting the criteria for defining mesenchymal stem cells (Figure 1D).

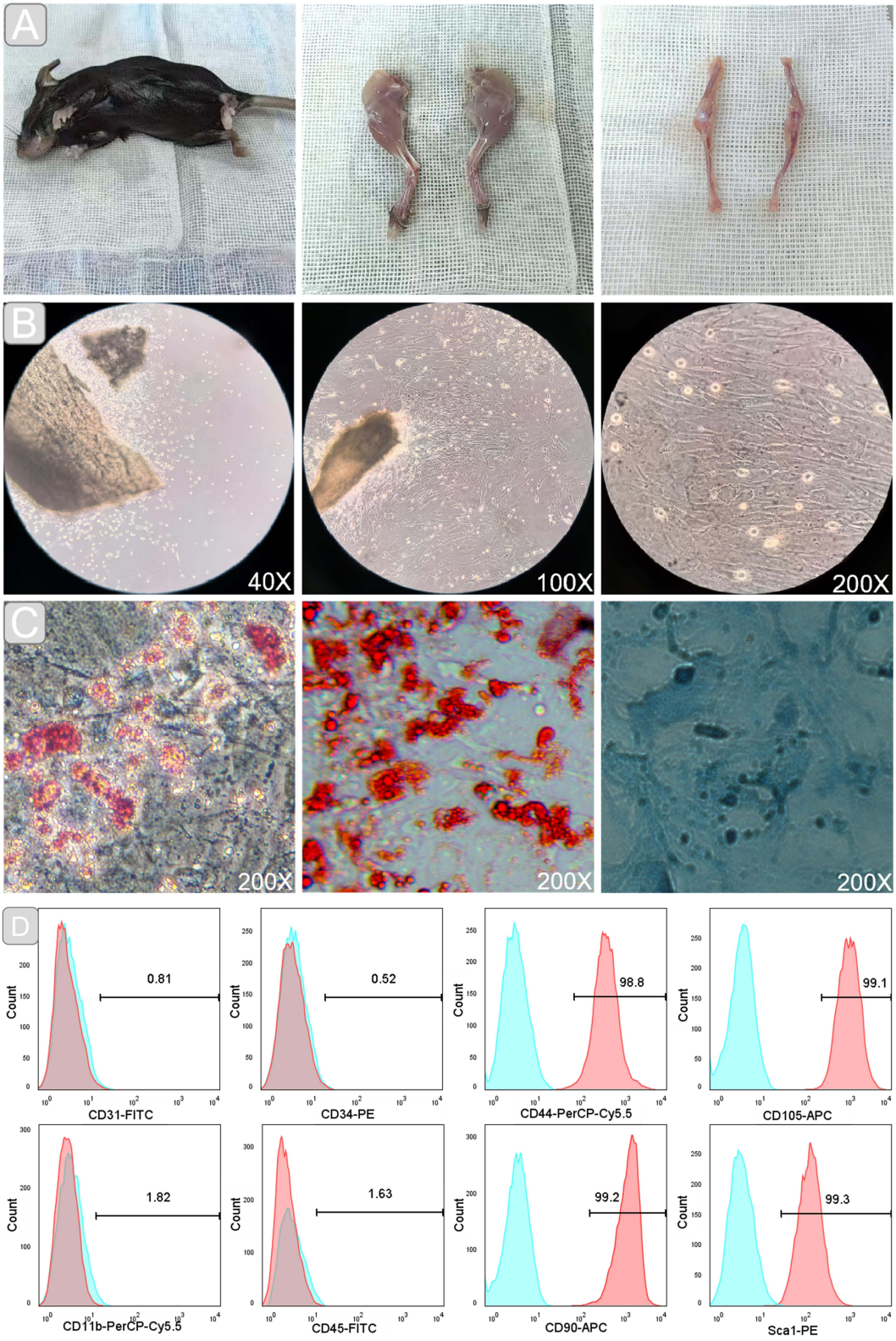

Figure 1 Characterization of bone marrow-derived mesenchymal stem cells (BMSCs). (**A**) Surgical isolation of mouse femoral and tibial bone chips for BMSC extraction using the compact bone digestion–explant method. (**B**) Phase-contrast microscopy showing fibroblast-like morphology and spiral colony formation by 10–14 days. (**C**) Trilineage differentiation confirmed by Alizarin Red S staining for osteogenesis, Oil Red O staining for adipogenesis, and Alcian Blue staining for chondrogenesis. (**D**) Flow cytometry analysis showing high expression of CD44, CD90, CD105, and Sca-1, and negative expression of CD31, CD34, CD45, and CD11b.

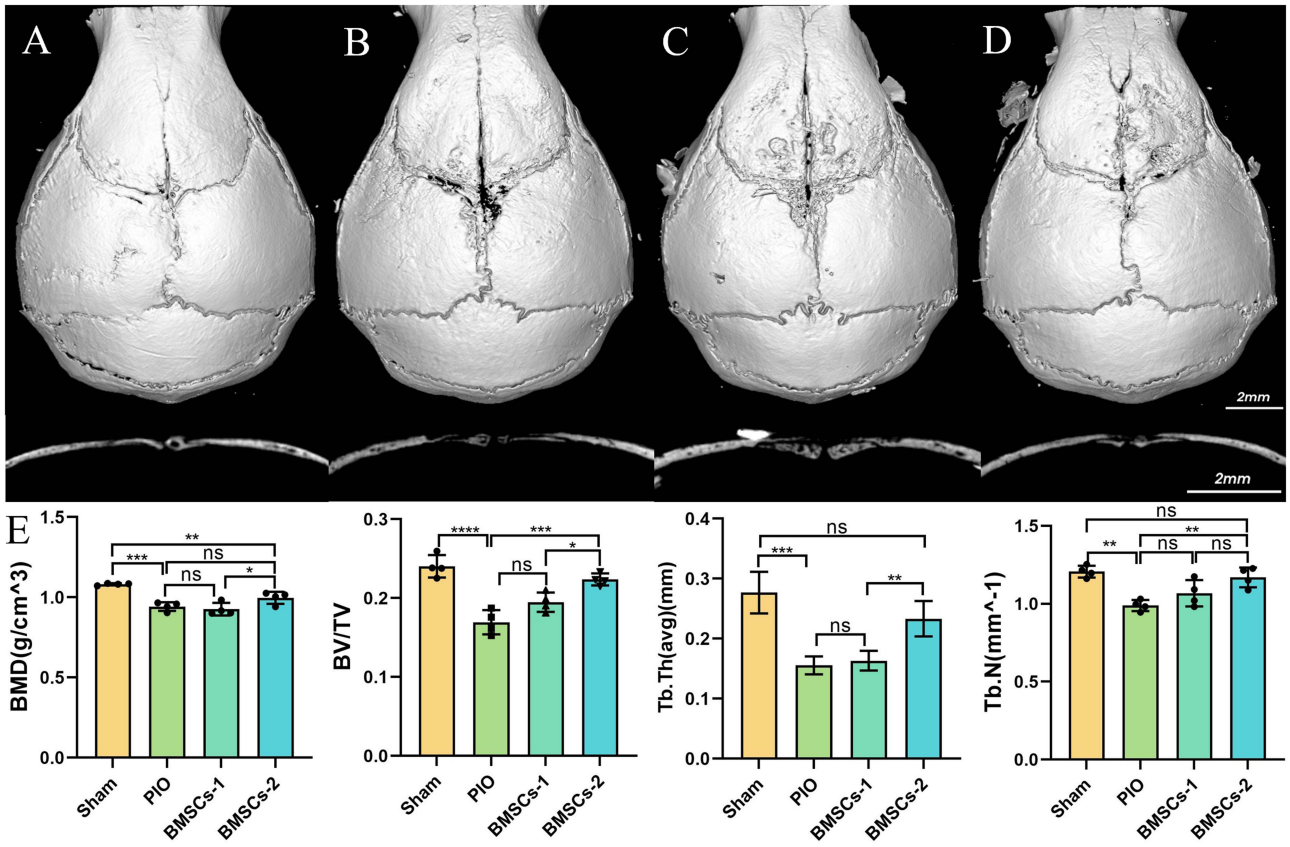

Figure 2 Micro-CT evaluation of UHMWPE particle-induced calvarial osteolysis and the effects of BMSC treatment. (**A–D**) Representative 3D micro-CT images of murine calvaria: Sham (**A**), PIO (**B**) single BMSC injection (BMSCs-1, C), and repeated injections (BMSCs-2, D). Bone resorption was observed in the PIO group and alleviated by BMSC therapy, especially in BMSCs-2. (**E**) Quantitative analysis of BMD, BV/TV, Tb.Th, and Tb.N showed significant improvement in bone quality after BMSC treatment compared with PIO. Data are mean ± SD (n = 4). *P < 0.05, **P < 0.01, ***P < 0.001, ****P < 0.0001 vs PIO.
Abbreviation: ns, not significant.

BMSCs Alleviate UHMWPE Particle-Induced Calvarial Osteolysis in vivo

To evaluate the therapeutic effects of BMSCs on UHMWPE particle-induced osteolysis, micro-CT was used to assess the calvarial bone loss. As shown in Figure 2A–D), group A (sham) displayed intact cortical bone and dense trabeculae, whereas group B (PIO model) showed severe cortical erosion and trabecular destruction. The C group (single BMSC injection, BMSCs-1) slightly reduced bone resorption but lacked clear structural restoration. In contrast, the D group (repeated BMSC injections, BMSCs-2) demonstrated more evident preservation of trabecular architecture.

The quantitative analysis (Figure 2E) confirmed these observations. UHMWPE particles significantly reduced BMD, BV/TV, and Tb. Th, and Tb. N compared to those in the sham (P<0.01–0.0001). A single BMSC injection did not produce significant improvements in any of these parameters. However, repeated BMSC delivery significantly increased BV/TV (P<0.05), Tb. Th (P<0.01), and Tb. N (P<0.05) compared to the B group, although BMD remained lower than that in the sham with only mild, non-significant recovery.

These findings suggest that repeated BMSC treatment alleviates UHMWPE-induced bone loss primarily by improving trabecular volume and architecture, whereas full mineral density recovery may require longer-term remodeling.

Histological and Immunohistochemical Evaluation of Calvarial Tissue

HE staining revealed marked periosteal thickening, dense inflammatory cell infiltration, and extensive bone surface erosion in the PIO group compared with the sham group (Figure 3A). In the BMSCs-1 injection group, periosteal hyperplasia and inflammatory infiltration were noticeably reduced, and more intact cortical bone could be observed.

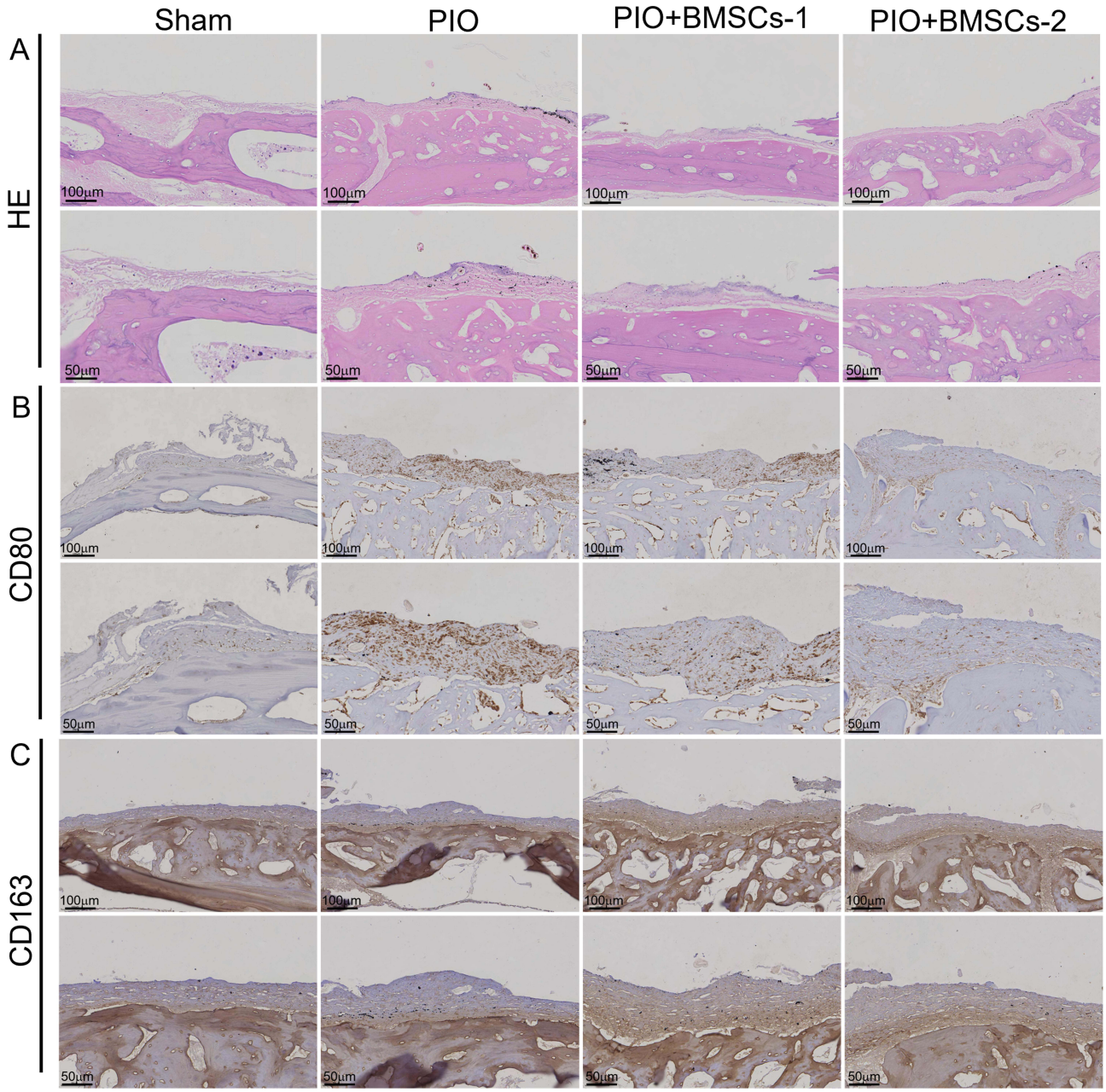

Figure 3 Histological and immunohistochemical staining of calvarial sections. (**A**) HE staining showing periosteal inflammation and bone destruction in the PIO group, partially alleviated by BMSC treatment. (**B**) IHC staining of CD80 showing reduced pro-inflammatory macrophage infiltration following single and repeated BMSC administration. (**C**) IHC staining of CD163 showing increased anti-inflammatory macrophage recruitment after BMSC treatment. Scale bars = 100 μm and 50 μm.

BMSCs-2 showed the greatest reduction in inflammatory infiltration and better preservation of bone architecture, with the periosteal morphology approaching that of the sham group.

IHC staining further demonstrated changes in macrophage polarization within periosteal tissue (Figure 3B). CD80 was strongly expressed in the PIO group, with numerous CD80+ cells distributed along the periosteal surface and within the inflammatory lesion. In the BMSCs-1 group, CD80 expression was reduced compared with that in the PIO group, and the BMSCs-2 group showed an even lower density of $CD80^{+}$ cells.

Conversely, CD163 expression was markedly reduced in the PIO group compared with that in the sham group (Figure 3C). BMSC treatment restored CD163 expression, with more CD163+ cells visible in both single and repeated-

injection groups. The BMSCs-2 group showed the most abundant CD163+ macrophage distribution, particularly around the preserved cortical bone.

Taken together, the histological and IHC staining results suggest that BMSC treatment alleviates UHMWPE-induced inflammatory bone destruction, suppresses M1 macrophage infiltration, and promotes M2 macrophage recruitment, with repeated injection providing a more pronounced effect.

BMSCs Modulate Periosteal Inflammatory Cytokines and Macrophage Polarization in vivo

BMSCs Enhance M2 Macrophage Polarization in Periosteal Tissue

Macrophage polarization in the calvarial periosteum was analyzed using flow cytometry. For CD80 (M1 macrophage marker), the proportion of CD80+ macrophages was 25.02 ± 2.00% in the sham group and increased markedly to 36.25 ± 2.86% in the PIO group ($P < 0.01$). Both BMSC-treated groups showed reduced CD80 expression relative to PIO, with values of 23.48 ± 4.48% in the BMSCs-1 group and 24.98 ± 2.52% in the BMSCs-2 group ($P < 0.01$ vs PIO) (Figure 4A).

The proportion of CD206+ (M2) macrophages was significantly lower in the PIO group (14.71 ± 2.65%) than in the sham (24.94 ± 3.33%, $P < 0.05$). Both BMSC-treated groups showed increased CD206 expression compared with PIO, reaching 24.07 ± 4.98% in BMSCs-1 and 25.40 ± 2.35% in BMSCs-2 ($P < 0.05$ for both vs PIO) (Figure 4B).

In addition, the CD80+/CD206+ polarization ratio (Figure 4C) was markedly elevated in the PIO group (1.64 ± 0.03) compared with the sham (1.20 ± 0.19, $P < 0.01$), indicating enhanced M1 polarization. This ratio was significantly reduced after BMSC treatment. This ratio decreased to 1.15 ± 0.02 and 1.12 ± 0.05 in the BMSCs-1 and BMSCs-2 groups, respectively, restoring values close to those observed in the sham. Representative flow cytometry plots (Figure 4D and E) further illustrate these changes, showing a clear rightward expansion of CD80+ M1 cells under UHMWPE stimulation, which was substantially reversed following BMSC administration, alongside an increase in CD206+ M2 macrophages.

BMSCs Regulate Periosteal Inflammatory Cytokine Levels

The periosteal tissue was analyzed by ELISA on day 21. TNF-α levels were significantly higher in the PIO group than in the sham ($P < 0.05$). Single BMSC treatment (BMSCs-1) slightly reduced TNF-α but without statistical significance, whereas repeated treatment (BMSCs-2) markedly suppressed TNF-α to near-sham levels ($P < 0.05$ vs PIO) (Figure 4F). For IL-10, the PIO group showed the highest levels ($P<0.05$ vs sham), indicating a compensatory anti-inflammatory response. BMSCs-1 slightly lowered IL-10 (ns), while BMSCs-2 significantly reduced IL-10 compared with PIO ($P<0.05$), reaching values comparable to those of sham (Figure 4G).

Overall, repeated BMSC administration more effectively modulated periosteal inflammation and suppressed excessive TNF-α production, while normalizing dysregulated IL-10.

UHMWPE Particles Induce Dose-Dependent Macrophage Polarization in vitro

RAW264.7 macrophages were exposed to UHMWPE particles at 0.05, 0.1, 0.2, and 0.8 mg/mL for 24 h, and M1 (CD80) and M2 (CD206) expression was analyzed by flow cytometry. Quantitative analysis (Figure 5A–C) showed that the proportion of F4/80+CD80+ (M1) macrophages significantly increased at 0.05, 0.1, and 0.2 mg/mL compared with control (****$P < 0.0001$, ***$P < 0.001$), while 0.8 mg/mL showed no significant difference. The proportion of F4/80 +CD206+ (M2) macrophages remained unchanged at lower concentrations but slightly increased at 0.8 mg/mL (*$P < 0.05$). The CD80+/CD206+ polarization ratio was maximally elevated at 0.05 and 0.1 mg/mL (****$P < 0.0001$), moderately at 0.2 mg/mL (***$P < 0.001$), and minimally at 0.8 mg/mL (**$P < 0.01$), indicating a dose-dependent shift toward M1 polarization. Representative flow cytometry plots (Figure 5D and E) illustrate these trends, showing an expansion of the CD80+ population with increasing particle concentrations and partial restoration of CD206+ expression at the highest dose.

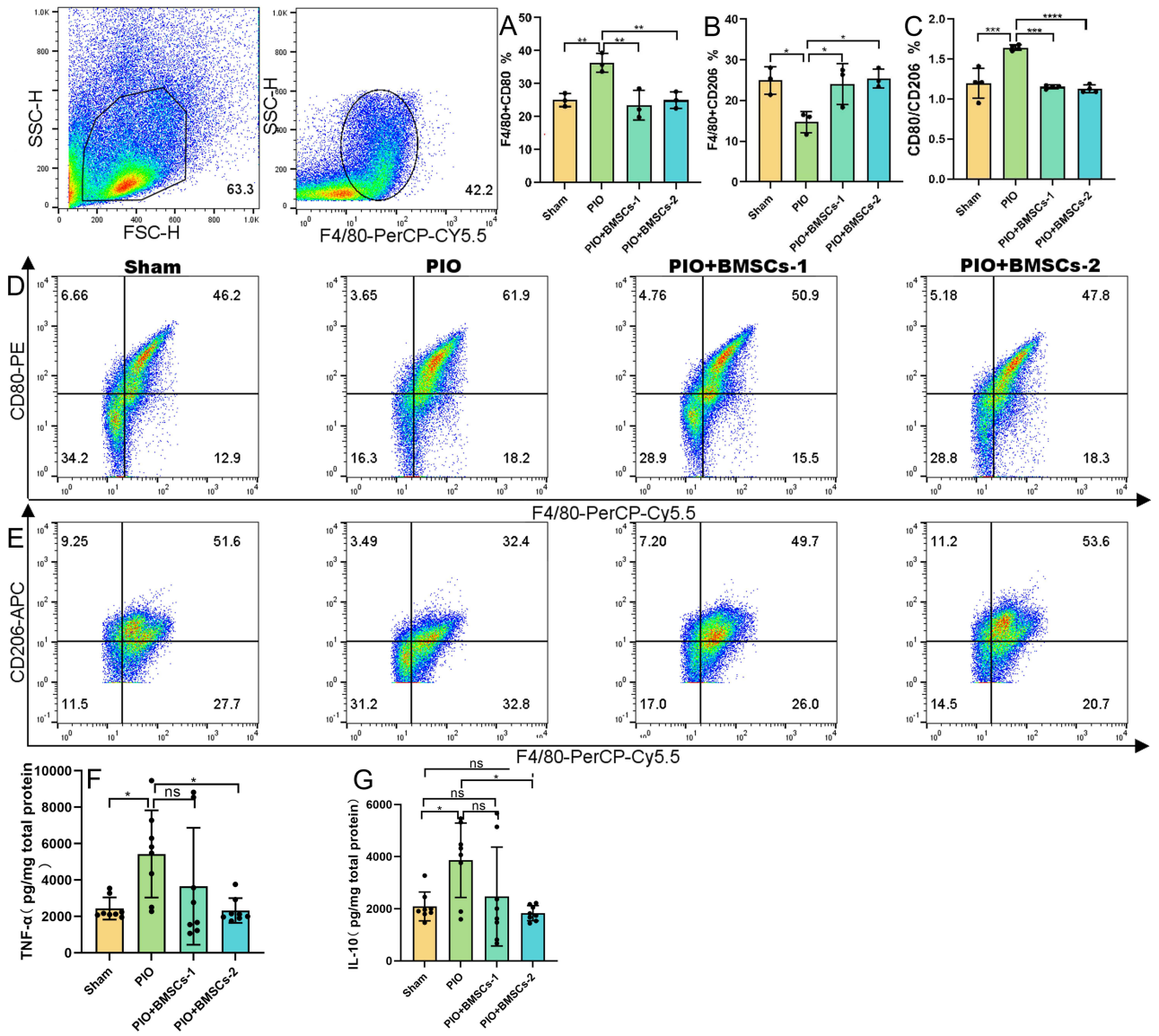

Figure 4 Flow cytometry and ELISA analyses of macrophage polarization and cytokine expression in periosteal tissue. (**A–C**) Quantitative analysis of CD80+ (M1) and CD206+ (M2) macrophages by flow cytometry showing increased CD80 and reduced CD206 in the PIO group, reversed by BMSC treatment, especially after repeated injections. (**D** and **E**) Representative gating plots illustrating M1/M2 distribution. (**F** and **G**) ELISA results showing elevated TNF-α and IL-10 in the PIO group and a reduction toward sham levels after BMSC therapy. Data are mean ± SD (n = 4). *P < 0.05, **P < 0.01, ***P < 0.001, ****P < 0.0001 vs PIO.
Abbreviation: ns, not significant.

Collectively, 0.2 mg/mL UHMWPE induced a stable and reproducible pro-inflammatory phenotype while maintaining macrophage viability, and was therefore selected for subsequent experiments.

BMSCs Suppress UHMWPE-induced Macrophage Polarization and Inflammatory Cytokines in vitro

BMSCs Modulate Macrophage Polarization in Vitro

Macrophage polarization in RAW264.7 cells was analyzed using flow cytometry after UHMWPE particle stimulation (Figure 6A–E). The proportion of CD80+ (M1) macrophages increased from 44.17 ± 2.79% in the RAW264.7 control group to 89.63 ± 0.46% after UHMWPE stimulation (P < 0.0001). BMSCs co-culture with UHMWPE significantly reduced CD80+ expression to 46.94 ± 8.57% (P < 0.0001 vs UHMWPE), restoring values close to the RAW264.7 control group baseline. For CD206+ (M2) macrophages, UHMWPE exposure caused only a minor change (10.40 ± 0.11% vs

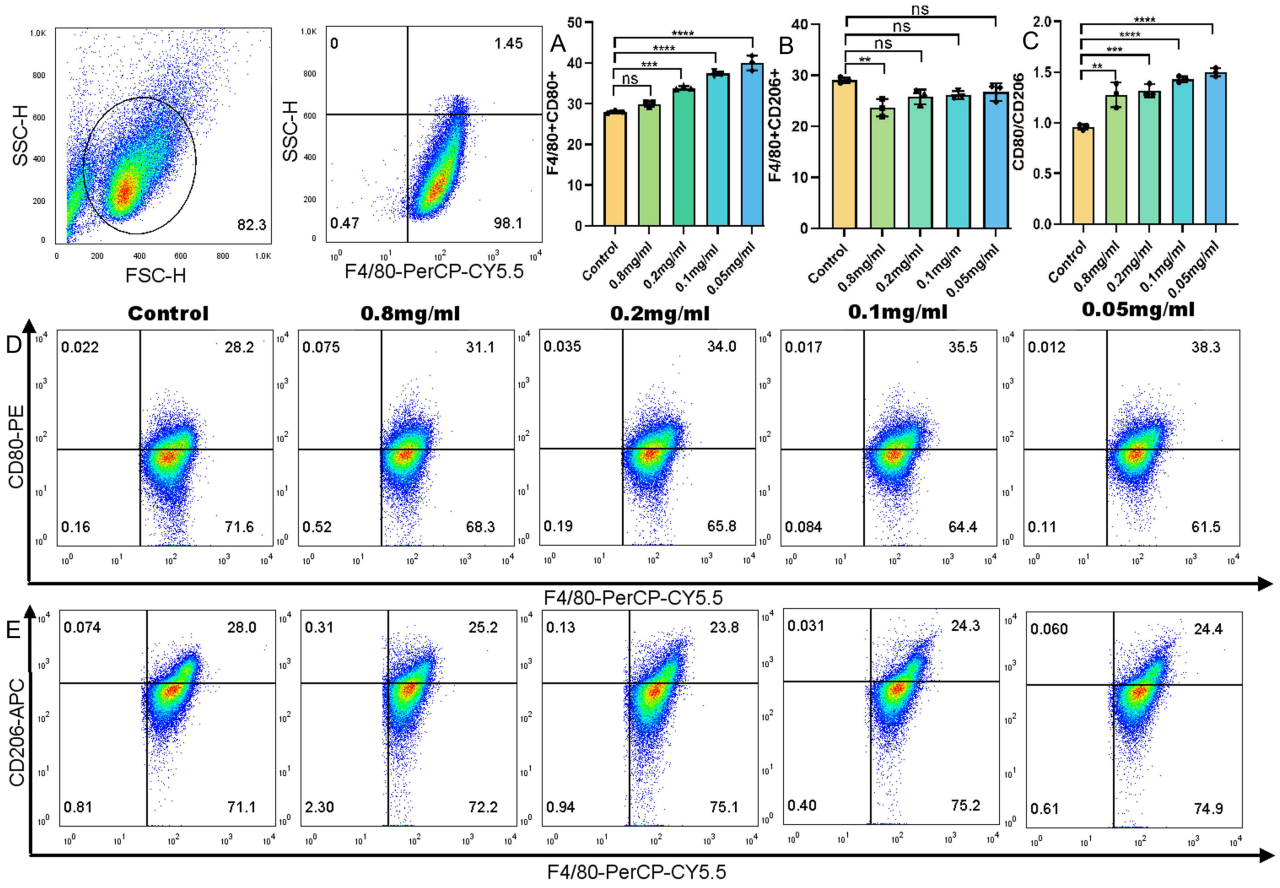

Figure 5 Dose-dependent effects of UHMWPE particles on macrophage polarization. (**A–C**) Quantification of CD80+, CD206+, and the M1/M2 ratio across particle concentrations, showing elevated M1 polarization and reduced M2 expression in a dose-dependent manner. (**D** and **E**) Representative flow cytometry plots of CD80 and CD206 expression. Data are presented as mean ± SD (n = 3). **P < 0.01, ***P < 0.001, ****P < 0.0001 vs control.
Abbreviation: ns, not significant.

12.25 ± 0.29% in control, ns), whereas BMSCs alone markedly increased CD206+ expression to 35.27 ± 0.91% (P < 0.0001 vs RAW264.7), and BMSCs co-culture with UHMWPE-stimulated macrophages further elevated CD206+ expression to 30.69 ± 2.48% (P < 0.0001 vs UHMWPE).

Consequently, the CD80+/CD206+ polarization ratio rose from 4.25 ± 0.31 in control to 7.32 ± 0.18 in the UHMWPE group (P < 0.0001), and was significantly reduced to 1.52 ± 0.17 by BMSC co-culture with UHMWPE (P < 0.0001 vs UHMWPE), indicating a clear restoration of the M1/M2 balance.

BMSCs Regulate Inflammatory Cytokine Secretion in vitro

ELISA analysis of culture supernatants (Figure 6F and G) showed that UHMWPE particles significantly elevated TNF-α compared with the RAW264.7 group (P < 0.0001), whereas BMSC co-culture markedly reduced TNF-α to near-baseline levels (P < 0.0001 vs UHMWPE). Conversely, IL-4 secretion was only slightly increased by UHMWPE particles, but was further enhanced by BMSC co-culture (P < 0.0001 vs UHMWPE).

Overall, these in vitro results demonstrate that BMSCs suppress UHMWPE-induced pro-inflammatory M1 polarization while promoting an anti-inflammatory M2 phenotype, accompanied by corresponding cytokine reprogramming.

BMSCs Modulate UHMWPE-Induced Macrophage Polarization by Immunofluorescence

Immunofluorescence staining revealed macrophage polarization under UHMWPE stimulation and BMSC co-culture (Figure 7). CD80 (green) indicates M1 macrophages, CD206 (green) indicates M2 macrophages, F4/80 (red) indicates all

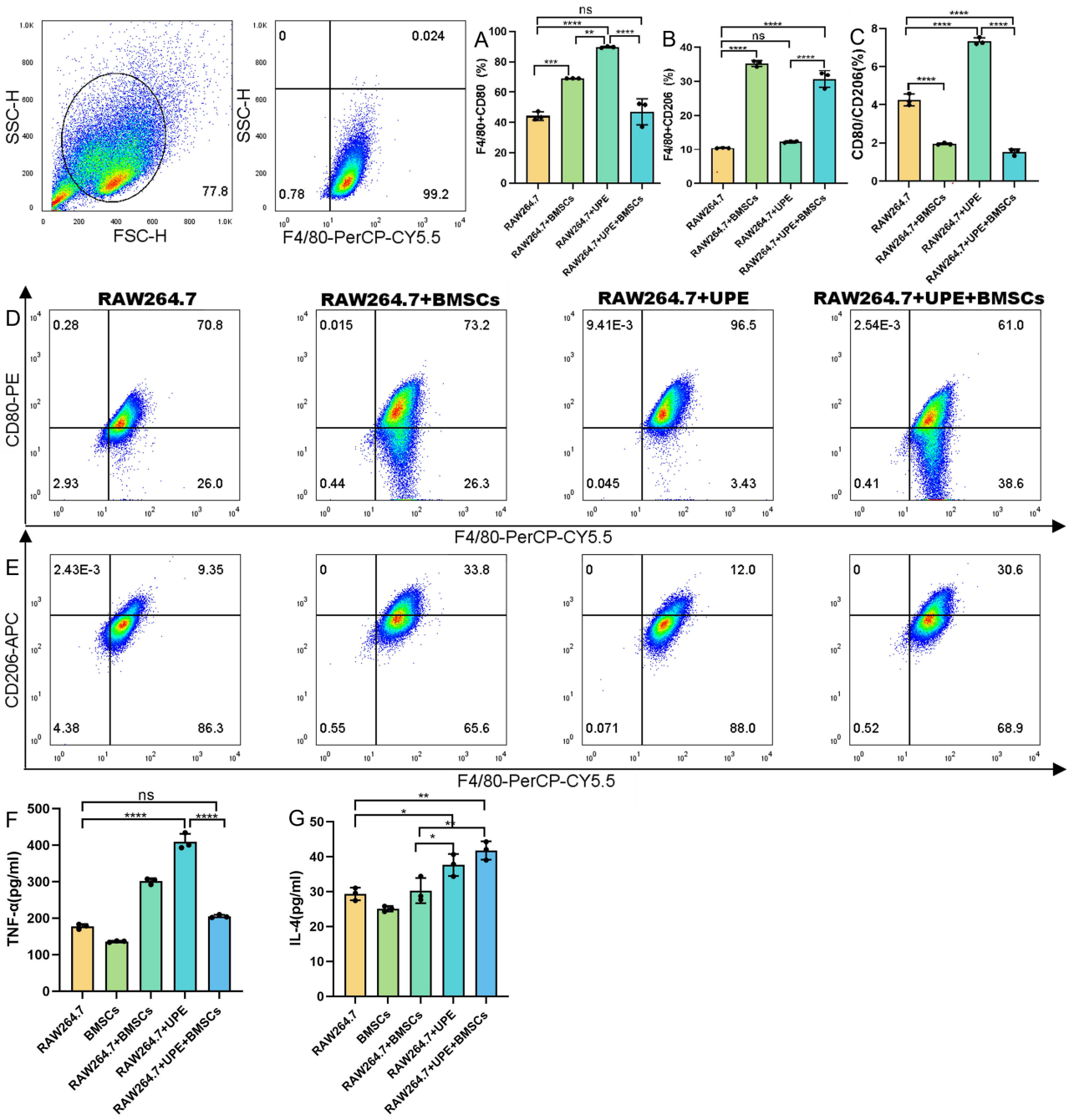

Figure 6 Effects of BMSCs on UHMWPE-induced macrophage polarization and cytokine secretion in vitro. (**A–C**) Quantitative analysis of F4/80+CD80+ (M1) and F4/80+CD206+ (M2) macrophages showing increased M1 and reduced M2 polarization after UHMWPE exposure, both reversed by BMSC co-culture. (**D** and **E**) Representative flow cytometry plots illustrating polarization shifts. (**F** and **G**) ELISA results showing UHMWPE-induced TNF-α elevation and mild IL-4 increase, both further modulated by BMSC co-culture. Data are mean ± SD (n = 3). *P < 0.05, **P < 0.01, ***P < 0.001, ****P < 0.0001 vs control.
Abbreviation: ns, not significant.

macrophage types, and DAPI (blue) indicates the nuclei. The groups included M (RAW264.7), M + UPE (RAW264.7 + UHMWPE), and M (UPE) + BMSCs (RAW264.7 + UHMWPE + BMSCs).

For CD80, the M group showed weak staining, indicating a resting state. The UHMWPE particles markedly increased the CD80 fluorescence, confirming M1 polarization. BMSC co-culture reduced CD80 staining compared to that in the M +UPE group, suggesting suppression of M1 activation. For CD206, baseline expression in the M group was moderate but

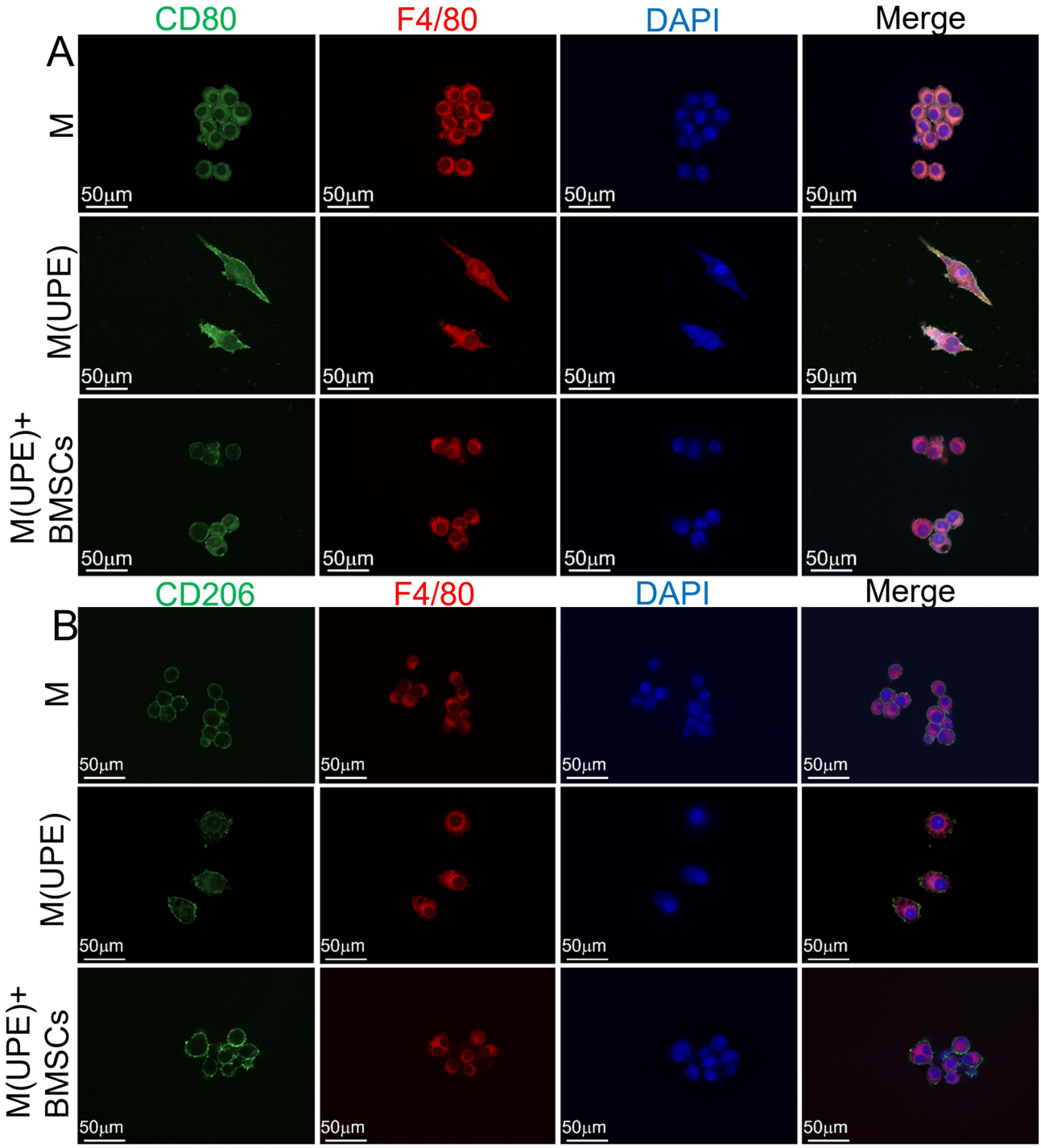

Figure 7 Immunofluorescence of macrophage polarization markers.(**A**) CD80 (green), F4/80 (red), and DAPI (blue) staining showed strong M1 marker expression in RAW264.7 + UHMWPE, reduced by BMSC co-culture. (**B**) CD206 (green), F4/80 (red), and DAPI (blue) staining were suppressed by UHMWPE but enhanced after BMSC co-culture. Scale bar: 50 μm.

further suppressed by UHMWPE particle, indicating reduced M2 polarization. Co-culture with BMSCs restored CD206 fluorescence, promoting a shift toward the M2 phenotype.

These qualitative observations align with the flow cytometry results, supporting BMSCs' role in reprogramming macrophages toward an anti-inflammatory state.

https://doi.org/10.2147/JIR.S557244

Discussion

Periprosthetic osteolysis remains the leading cause of late implant failure and is primarily driven by macrophage-mediated inflammation in response to wear particles.[16,40] Among these, UHMWPE debris is clinically more relevant than titanium because of its higher generation rate in modern prostheses. This paper further indicates that UHMWPE particles elicit stronger sex-dependent macrophage responses than metallic debris, resulting in more persistent inflammation.[41] In our study, UHMWPE particles induced robust M1 macrophage polarization, elevated TNF-α, and significant bone loss, confirming previous findings that particulate debris skews macrophages toward a pro-inflammatory phenotype.[42,43]

Consistent with prior studies on wear particle–induced osteolysis, our data demonstrated that UHMWPE particles strongly promote M1 macrophage polarization and pro-inflammatory cytokine secretion. Similar inflammatory profiles have been observed in titanium and nanoparticle exposure models, confirming macrophage activation as a key pathogenic mechanism in periprosthetic osteolysis.[44]

However, our results extend these findings by showing that UHMWPE particles not only trigger stronger pro-inflammatory activation than metallic debris but also induce a dysregulated compensatory IL-10 response, suggesting sustained immune stress rather than transient inflammation. Importantly, repeated administration of BMSCs effectively alleviated bone destruction, reduced TNF-α levels, and enhanced M2 macrophage polarization both in vivo and in vitro.

The RAW264.7 murine macrophage line, as used in our study, is a well-established in vitro model owing to its stable genotype, consistent phenotype, and reproducible responsiveness to immune stimuli, such as lipopolysaccharides (LPS).[45] These cells retain key macrophage functions, including phagocytosis, nitric oxide production, and cytokine secretion, which closely mirror the behavior of primary macrophages under inflammatory stress.[46] This supports their reliability in modeling wear particle–induced immune responses and osteolytic processes.

UHMWPE Particles Induce Persistent M1 Polarization and Dysregulated IL-10

UHMWPE particles caused a pronounced increase in CD80+ macrophages and TNF-α secretion, consistent with evidence that wear debris activates NF-κB and MAPK signaling, amplifying osteoclastogenesis.[47,48] Indeed, UHMWPE debris specifically activates the Chemerin/ChemR23–NF-κB axis, amplifying downstream AP-1 signaling and sustaining TNF-α release.[49,50] Interestingly, IL-10, a classical anti-inflammatory cytokine, was also elevated in the particle-stimulated periosteum. Similar paradoxical IL-10 upregulation has been reported in UHMWPE particle-induced osteolysis models as a transient compensatory response attempting to counterbalance TNF-α-driven inflammation.[51]

Specifically, Loi demonstrated that UHMWPE-induced macrophage activation leads to simultaneous TNF-α and IL-10 secretion, reflecting a mixed but imbalanced immune state.[52] Likewise, a murine UHMWPE model revealed that while TNF-α and IL-6 are strongly induced, IL-10 also increases at sub-compensatory levels—a response further modulated by metformin treatment.[51] However, these endogenous IL-10 responses remain insufficient to restore immune balance, as the M1/M2 ratio stays skewed, sustaining osteoclast-driven bone resorption.[20]

Interestingly, our study also revealed that IL-10 levels decreased following BMSC treatment, concurrent with the reduction of TNF-α. This seemingly paradoxical pattern likely reflects the self-limiting nature of the IL-10 response. During intense inflammatory activation, macrophages upregulate IL-10 as a negative feedback mechanism through STAT3-dependent induction of SOCS3, aiming to restrain excessive NF-κB signaling.[53,54] However, once the inflammatory drive subsides—such as after BMSC-mediated suppression of TNF-α and restoration of M2 polarization—the stimulus for IL-10 production is reduced, leading to normalization rather than persistent elevation.[54] In mathematical models of LPS-stimulated monocytes, IL-10 expression similarly peaks early and declines as pro-inflammatory signaling wanes.[55] Moreover, in wear particle–induced osteolysis, the NF-κB/let-7f-5p–IL-10 pathway has been shown to regulate macrophage polarization, where let-7f-5p suppresses IL-10 expression and reinforces M1 activation.[56] Moreover, macrophage models have demonstrated that IL-10 transcription can be initiated within minutes but is transient and subject to remodeling.[57] Collectively, these findings indicate that IL-10 expression is dynamically tuned by feedback circuits and does not remain persistently elevated once inflammatory homeostasis is restored.[58]

Our flow cytometry and ELISA data confirmed a significant rise in CD80+ macrophages, supporting a model-dependent inflammatory shift. These findings reinforce the idea that wear particles generate a “mixed but predominantly

pro-inflammatory" immune microenvironment, where IL-10 is present but insufficient to counteract the dominant M1-mediated inflammatory cascade.

BMSCs Reprogram Macrophage Phenotypes and Modulate Cytokines

BMSC co-culture significantly suppressed M1 polarization while promoting M2 differentiation, as shown by decreased CD80 and increased CD206 expression. This aligns with previous studies demonstrating that BMSCs exert immunosuppressive effects through paracrine secretion of prostaglandin E2 (PGE2), TSG-6, IL-10, and TGF-β, which inhibit NF-κB activation and promote STAT3 signaling.[29,59] Notably, repeated BMSC administration in vivo achieved more pronounced effects than a single injection, likely due to enhanced local retention and sustained release of immunomodulatory factors.[60] Similar trends were observed in rheumatoid arthritis and bone defect models, where multiple BMSC doses improved therapeutic efficacy compared with single dosing.[34,61]

Immunofluorescence further confirmed these effects: UHMWPE-stimulated macrophages showed intense CD80 fluorescence colocalizing with F4/80, whereas BMSC co-culture markedly reduced this signal. Conversely, CD206 fluorescence, which was suppressed by UHMWPE, was restored by BMSCs treatment. These findings support the idea that BMSC-derived soluble factors and extracellular vesicles directly drive macrophage phenotype switching.[23,28]

Mechanistic Insights and Emerging Pathways

Based on our flow cytometry and ELISA findings showing a marked TNF-α reduction but normalized IL-10 levels after BMSC treatment, we speculate that BMSCs restore immune homeostasis through the NF-κB/STAT3 feedback network rather than merely amplifying M2 polarization. Besides classical NF-κB inhibition, recent work suggests IL-17 signaling and ferroptosis contribute to particle-induced osteolysis.[62] Interestingly, some studies link IL-17 to LCN2-mediated chronic inflammation and bone loss, raising the possibility that IL-17/LCN2 signaling might underlie the "mixed but imbalanced" immune state we observed.[63,64] In our model, UHMWPE stimulation caused robust TNF-α secretion accompanied by a compensatory but insufficient IL-10 elevation, suggesting a prolonged low-level inflammatory stress rather than acute necrotic damage, which is consistent with ferroptosis-associated chronic macrophage injury reported in wear debris models.[65] Although we did not directly detect ferroptosis markers, the partial restoration of M2 macrophages after BMSC treatment implies their action may converge on rebalancing NF-κB/STAT3 rather than completely blocking IL-17 signaling. Furthermore, BMSC-derived exosomal miR-146a has been shown to suppress TRAF6/NF-κB, facilitating macrophage repolarization toward M2.[60,66]

Compared to titanium debris, UHMWPE particles induced both stronger TNF-α production and compensatory IL-10 elevation. This aligns with reports that UHMWPE debris preferentially activates monocyte/macrophage-mediated inflammation with limited lymphocyte involvement, whereas metallic debris triggers a broader innate and adaptive immune response due to ion release and oxidative stress.[67] Therefore, the type of wear particle may influence the required immunomodulatory strategy.

Translational Relevance

Our study adds two clinically meaningful insights: (1) UHMWPE-induced PPO requires prolonged immune regulation because particle release is chronic; (2) repeated BMSC delivery yields superior bone preservation compared with single dosing. Compared with single-target approaches such as surface-modified titanium implants or small-molecule anti-inflammatory drugs, BMSCs exhibit a dual advantage by simultaneously regulating immune polarization and promoting osteogenic microenvironments, which may explain the superior bone preservation observed with repeated dosing. This supports the concept of optimized BMSC treatment schedules or cell-free therapies using preconditioned exosomes as a future direction. The latest USC-derived exosome and MSC-EV therapies showed immunomodulatory efficacy equivalent to that of live MSCs, suggesting engineered EVs could reduce the need for repeated cell transplantation.[68,69] Exosome-based therapies offer several practical advantages over direct stem cell transplantation, including their "off-the-shelf" availability, absence of tumorigenic or differentiation risks, greater stability during storage and transport, and easier standardization for clinical manufacturing.[70,71] These features make exosome therapy an attractive and scalable alternative for translational applications in orthopedic and inflammatory bone diseases.

By combining in vivo periosteal macrophage flow cytometry, cytokine assays, and in vitro transwell co-culture, we provided multi-layer evidence of BMSC-driven macrophage reprogramming. Few PPO studies integrate these complementary approaches, making this work more comprehensive in evaluating immune–bone crosstalk.

Limitations and Future Directions

This study has some limitations. First, the 21-day observation period may not capture long-term remodeling, as bone mineral density recovery lagged behind trabecular structure restoration. Second, we did not directly trace BMSC survival or exosome release at the calvarial site. Advanced tools, such as single-cell RNA sequencing and live-cell tracking, can clarify the temporal dynamics of macrophage reprogramming. Third, although previous studies have implicated NF κB, TLR4/MyD88, ferroptosis-related NF κB-SLC7A11, and chemerin/ChemR23-AP 1 signaling in wear particle-induced immune dysregulation, this study did not directly investigate the underlying signaling pathways, which is a notable limitation; nevertheless, subsequent research is planned to elucidate these mechanisms in detail.

Additionally, exploring BMSC-derived exosomes as a cell-free alternative may overcome logistical barriers to repeated cell transplantation.[72] Compared with live cell delivery, exosome-based approaches offer improved delivery consistency, lower immunogenicity, and reduced safety risks associated with uncontrolled differentiation or vascular occlusion.[73] Future studies could leverage engineered BMSCs or bone-targeting exosomes (eg, collagen-binding EVs) to achieve "low-dose, high-efficiency" or sustained release, thereby enhancing therapeutic precision and reproducibility while maintaining safety and controllability. Finally, validating these findings in larger, load-bearing models is essential for clinical translation.

Conclusion

This study demonstrates that local delivery of bone marrow mesenchymal stem cells (BMSCs), particularly through repeated administration, effectively attenuates UHMWPE wear particle–induced osteolysis by reprogramming macrophage polarization from a pro-inflammatory (M1) to an anti-inflammatory (M2) phenotype. We confirmed that BMSCs exert these effects mainly via paracrine-mediated immune modulation, leading to reduced cytokine secretion and improved bone microarchitecture. These findings provide a mechanistic foundation for developing MSC-based immunomodulatory therapies against periprosthetic osteolysis and related inflammatory bone disorders.

Despite these promising results, further studies are required to address current challenges, including long-term efficacy, detailed signaling mechanisms, and optimization of delivery strategies. Future work focusing on BMSC-derived exosomes and bone-targeted cell-free systems may offer a more practical, safe, and scalable therapeutic approach for clinical translation.

Abbreviations

PPO, periprosthetic osteolysis; UHMWPE, ultra-high molecular weight polyethylene; BMSCs, bone marrow mesenchymal stem cells; TJA, total joint arthroplasty; HE staining, hematoxylin and eosin staining; IHC, immunohistochemical; ELISA, enzyme-linked immunosorbent assay; IF, immunofluorescence; BMD, bone mineral density; BV/TV, bone volume fraction/total volume; TNF-α, tumor necrosis factor alpha; Tb.Th, trabecular thickness; Tb.N, trabecular number; IL-10, Interleukin-10; IL-4, Interleukin-4.

Data Sharing Statement

The data that support the findings of this study are available from the corresponding author upon reasonable request.

Ethics State

All animal procedures were reviewed and approved by the Ethics Committee of the First Affiliated Hospital of Harbin Medical University. The study strictly followed the National Research Council's Guide for the Care and Use of Laboratory Animals.

Author Contributions

All authors made a significant contribution to the work reported, whether that is in the conception, study design, execution, acquisition of data, analysis and interpretation, or in all these areas; took part in drafting, revising or critically reviewing the article; gave final approval of the version to be published; have agreed on the journal to which the article has been submitted; and agree to be accountable for all aspects of the work.

Funding

The authors report no funding associated with the study described in this article.

Disclosure

The author(s) report no conflicts of interest in this work.

References

1. Matsumae G, Shimizu T, Tian Y, et al. Targeting thymidine phosphorylase as a potential therapy for bone loss associated with periprosthetic osteolysis. *Bioengineer Transl Med*. 2021;6(3):e10232. doi:10.1002/btm2.10232
2. Meng J, Zhou C, Hu B, et al. Stevioside prevents wear particle-induced osteolysis by inhibiting osteoclastogenesis and inflammatory response via the suppression of TAK1 activation. *Front Pharmacol*. 2018;9:1053. doi:10.3389/fphar.2018.01053
3. Ren Y, Zhang Y, Wang Z, et al. Role of Brd4 in the production of inflammatory cytokines in mouse macrophages treated with titanium particles. *Canadian J Physiol Pharmacol*. 2019;97(11):1028–1034. doi:10.1139/cjpp-2019-0142
4. Lin S, Wen Z, Li S, et al. LncRNA *Neat1* promotes macrophage inflammatory responses and acts as a therapeutic target in titanium particle-induced osteolysis. *SSRN Electronic J*. 2021. doi:10.2139/ssrn.3943649
5. Oral E, Greenbaum ES, Malhi AS, Harris WH, Muratoglu OK. Characterization of irradiated blends of alpha-tocopherol and UHMWPE. *Biomaterials*. 2005;26(33):6657–6663. doi:10.1016/j.biomaterials.2005.04.026
6. Yang C, Li J, Zhu K, et al. Puerarin exerts protective effects on wear particle-induced inflammatory osteolysis. *Front Pharmacol*. 2019;10:1113. doi:10.3389/fphar.2019.01113
7. Silva-Bermudez LS, Sevastyanova TN, Schmuttermaier C, et al. Titanium nanoparticles enhance production and suppress stabilin-1-mediated clearance of GDF-15 in human primary macrophages. *Front Immunol*. 2021;12. doi:10.3389/fimmu.2021.760577
8. Yap E, Wei J, Webb C, Ng K, Behrends M. Neuraxial and general anesthesia for outpatient total joint arthroplasty result in similarly low rates of major perioperative complications: a multicentered cohort study. *Regional Anesthesia Pain Med*. 2022;47(5):294–300. doi:10.1136/rapm-2021-103189
9. Shichman I, Roof M, Askew N, et al. Projections and epidemiology of primary hip and knee arthroplasty in medicare patients to 2040-2060. *JB JS Open Access*. 2023;8(1). doi:10.2106/jbjs.Oa.22.00112
10. Kurtz S, Ong K, Lau E, Mowat F, Halpern M. Projections of primary and revision hip and knee arthroplasty in the United States from 2005 to 2030. *J Bone Joint Surg*. 2007;89(4):780–785. doi:10.2106/jbjs.F.00222
11. Sloan M, Premkumar A, Sheth NP. Projected volume of primary total joint arthroplasty in the U.S. 2014 to 2030. *J Bone Joint Surg Am Vol*. 2018;100(17):1455–1460. doi:10.2106/jbjs.17.01617
12. Moldovan F, Moldovan L. A modeling study for hip fracture rates in Romania. *J Clin Med*. 2025;14(9):3162.
13. Bradaschia-Correa V, Josephson AM, Mehta D, et al. The selective serotonin reuptake inhibitor fluoxetine directly inhibits osteoblast differentiation and mineralization during fracture healing in mice. *J Bone Mineral Res*. 2017;32(4):821–833. doi:10.1002/jbmr.3045
14. Zhou Y, Hu Z, Ge M, et al. Intraosseous injection of calcium phosphate polymer-induced liquid precursor increases bone density and improves early implant osseointegration in ovariectomized rats. *Int J Nanomedicine*. 2021;16:6217–6229. doi:10.2147/ijn.S321882
15. Wang W, Wu C, Tian B, et al. The inhibition of RANKL-induced osteoclastogenesis through the suppression of p38 signaling pathway by naringenin and attenuation of titanium-particle-induced osteolysis. *Int J Mol Sci*. 2014;15(12):21913–21934. doi:10.3390/ijms151221913
16. Zheng K, Bai J, Li N, et al. Protective effects of sirtuin 3 on titanium particle-induced osteogenic inhibition by regulating the NLRP3 inflammasome via the GSK-3β/β-catenin signalling pathway. *Bioact Mater*. 2021;6(10):3343–3357. doi:10.1016/j.bioactmat.2021.02.039
17. Kartikasari N, Yamada M, Watanabe J, et al. Titanium surface with nanospikes tunes macrophage polarization to produce inhibitory factors for osteoclastogenesis through nanotopographic cues. *Acta Biomaterialia*. 2022;137:316–330. doi:10.1016/j.actbio.2021.10.019
18. Eger M, Hiram-Bab S, Liron T, et al. Mechanism and prevention of titanium particle-induced inflammation and osteolysis. *Front Immunol*. 2018;9:2963.
19. Pajarinen J, Kouri V-P, Jämsen E, T-F L, Mandelin J, Konttinen YT. The response of macrophages to titanium particles is determined by macrophage polarization. *Acta Biomaterialia*. 2013;9(11):9229–9240. doi:10.1016/j.actbio.2013.06.027
20. Jiang H, Wang Y, Tang Z, et al. Calycosin alleviates titanium particle-induced osteolysis by modulating macrophage polarization and subsequent osteogenic differentiation. *J Cell Mol Med*. 2024;28(7):e18157. doi:10.1111/jcmm.18157
21. Ge YW, Feng K, Liu XL, et al. Quercetin inhibits macrophage polarization through the p-38α/β signalling pathway and regulates OPG/RANKL balance in a mouse skull model. *J Cell Mol Med*. 2020;24(5):3203–3216. doi:10.1111/jcmm.14995
22. Lu H-L, Huang X-Y, Luo Y-F, Tan W-P, Chen P-F, Guo Y-B. Activation of M1 macrophages plays a critical role in the initiation of acute lung injury. *Bioscience Reports*. 2018;38(2). doi:10.1042/bsr20171555
23. Shapouri-Moghaddam A, Mohammadian S, Vazini H, et al. Macrophage plasticity, polarization, and function in health and disease. *Journal of Cellular Physiology*. 2018;233(9):6425–6440. doi:10.1002/jcp.26429

24. Wang L, Wang Q, Wang W, et al. Harmine alleviates titanium particle-induced inflammatory bone destruction by immunomodulatory effect on the macrophage polarization and subsequent osteogenic differentiation. *Frontiers in Immunology*. 2021;12. doi:10.3389/fimmu.2021.657687
25. van Hengel IAJ, Gelderman FSA, Athanasiadis S, et al. Functionality-packed additively manufactured porous titanium implants. *Materials Today Bio*. 2020;7:100060. doi:10.1016/j.mtbio.2020.100060
26. Abaricia JO, Shah AH, Ruzga MN, Olivares-Navarrete R. Surface characteristics on commercial dental implants differentially activate macrophages in vitro and in vivo. *Clinical Oral Implants Research*. 2021;32(4):487–497. doi:10.1111/clr.13717
27. Zhang G, Pan R, Lai S, et al. Phosphatidylserine-functional polydimethylsiloxane substrates regulate macrophage M2 polarization via modulus-dependent NF-κB/PPARγ pathway. *Biomaterials Advances*. 2024;165:213997. doi:10.1016/j.bioadv.2024.213997
28. Yang F, Li W-B, Qu Y-W, et al. Bone marrow mesenchymal stem cells induce M2 microglia polarization through PDGF-AA/MANF signaling. *World Journal of Stem Cells*. 2020;12(7):633–658. doi:10.4252/wjsc.v12.i7.633
29. Zhang Y, Liu L, Wang X, Shen X, Pei Y, Liu Y. Bone marrow mesenchymal stem cells suppress activated CD4+ T cells proliferation through TGF-beta and IL10 dependent of autophagy in pathological hypoxic microenvironment. *Biochemical and Biophysical Research Communications*. 2024;702:149591. doi:10.1016/j.bbrc.2024.149591
30. Geng J, G-Y L, Shu LS, Zhou H-Y. Effect and mechanism of treating experimental autoimmune encephalomyelitis in mice with butylphthalide combined with bone marrow mesenchymal stem cells. *Sichuan da xue xue bao Yi xue ban*. 2021;52:759–766. doi:10.12182/20210960206
31. Niemeyer P, Szalay K, Luginbühl R, Südkamp NP, Kasten P. Transplantation of human mesenchymal stem cells in a non-autogenous setting for bone regeneration in a rabbit critical-size defect model. *Acta Biomater*. 2010;6(3):900–908. doi:10.1016/j.actbio.2009.09.007
32. Li B, He X, Dong Z, et al. Ionomycin ameliorates hypophosphatasia via rescuing alkaline phosphatase deficiency-mediated L-type Ca(2+) channel internalization in mesenchymal stem cells. *Bone Research*. 2020;8:19. doi:10.1038/s41413-020-0090-7
33. Priya PS, Nayak SPRR, Margesan T, et al. Investigating the osteoprotective effects of quercetin and rutin from Terminalia chebula in glucocorticoid-induced osteoporosis in vitro cell line and in vivo zebrafish model. *South African Journal of Botany*. 2024;175:712–722. doi:10.1016/j.sajb.2024.10.060
34. Gao J, Zhang G, Xu K, et al. Bone marrow mesenchymal stem cells improve bone erosion in collagen-induced arthritis by inhibiting osteoclasia-related factors and differentiating into chondrocytes. *Stem Cell Research & Therapy*. 2020;11(1):171. doi:10.1186/s13287-020-01684-w
35. Zhang Y, Hao Z, Wang P, et al. Exosomes from human umbilical cord mesenchymal stem cells enhance fracture healing through HIF-1α-mediated promotion of angiogenesis in a rat model of stabilized fracture. *Cell Proliferation. Mar*. 2019;52(2):e12570. doi:10.1111/cpr.12570
36. Green TR, Fisher J, Matthews JB, Stone MH, Ingham E. Effect of size and dose on bone resorption activity of macrophages by in vitro clinically relevant ultra high molecular weight polyethylene particles. *Journal of Biomedical Materials Research*. 2000;53(5):490–497. doi:10.1002/1097-4636(200009)53:5<490::aid-jbm7>3.0.co;2-7
37. Liu A, Richards L, Bladen CL, Ingham E, Fisher J, Tipper JL. The biological response to nanometre-sized polymer particles. *Acta Biomater*. 2015;23:38–51. doi:10.1016/j.actbio.2015.05.016
38. Soleimani M, Nadri S. A protocol for isolation and culture of mesenchymal stem cells from mouse bone marrow. *Nature Protocols*. 2009;4(1):102–106. doi:10.1038/nprot.2008.221
39. Zhu H, Guo Z-K, Jiang -X-X, et al. A protocol for isolation and culture of mesenchymal stem cells from mouse compact bone. *Nature Protocols*. 2010;5(3):550–560. doi:10.1038/nprot.2009.238
40. Wu Y, Teng Y, Zhang C, et al. The ketone body β-hydroxybutyrate alleviates CoCrMo alloy particles induced osteolysis by regulating NLRP3 inflammasome and osteoclast differentiation. *J Nanobiotechnol*. 2022;20(1):120. doi:10.1186/s12951-022-01320-0
41. Landgraeber S, Samelko L, McAllister K, Putz S, Jacobs JJ, Hallab NJ. UHMWPE particulate implant debris induces sex dependent aseptic osteolysis responses in vivo using a murine model. *Open Orthopaedics J*. 2018;12(1):115–124. doi:10.2174/1874325001812010115
42. Wang X, Li Y, Feng Y, Cheng H, Li D. Macrophage polarization in aseptic bone resorption around dental implants induced by Ti particles in a murine model. *J Periodontal Res*. 2019;54(4):329–338. doi:10.1111/jre.12633
43. Song J, Chao J, Hu X, et al. E3 ligase FBXW7 facilitates mycobacterium immune evasion by modulating TNF-α expression. *Front Cell Infect Microbiol*. 2022;12:851197. doi:10.3389/fcimb.2022.851197
44. Wang W, Liang X, Liu X, et al. NOX4 blockade suppresses titanium nanoparticle-induced bone destruction via activation of the Nrf2 signaling pathway. *J Nanobiotechnol*. 2022;20(1):241. doi:10.1186/s12951-022-01413-w
45. Szliszka E, Skaba D, Czuba ZP, Krol W. Inhibition of inflammatory mediators by neobavaisoflavone in activated RAW264.7 macrophages. *Molecules*. 2011;16(5):3701–3712. doi:10.3390/molecules16053701
46. Raja Namasivayam SK, Venkatachalam G, Arvind Bharani RS. Immuno biocompatibility and anti-quorum sensing activities of chitosan-gum acacia gold nanocomposite (CS-GA-AuNC) against Pseudomonas aeruginosa drug-resistant pathogen. *Sustainable Chem Pharm*. 2020;17:100300. doi:10.1016/j.scp.2020.100300
47. Ingham E, Fisher J. Biological reactions to wear debris in total joint replacement. *Proceed Institut Mechanical Engineers Part H*. 2000;214(1):21–37. doi:10.1243/0954411001535219
48. Jia Q, Liu L, Yu Y, et al. Inhibition of EGFR pathway suppresses M1 macrophage polarization and osteoclastogenesis, mitigating titanium particle-induced bone resorption. *J Inflammation Res*. 2024;17:9725–9742. doi:10.2147/jir.S484529
49. Hu K, Shang Z, Yang X, Zhang Y, Cao LJJo IR. Macrophage polarization and the regulation of bone immunity in bone homeostasis. *J Inflammation Res*. 2023;3563–3580.
50. Zhao F, Cang D, Zhang J, Zheng LJAo TM. Chemerin/ChemR23 signaling mediates the effects of ultra-high molecular weight polyethylene wear particles on the balance between osteoblast and osteoclast differentiation. *Ann Transl Med*. 2021;9(14):1149.
51. Yan Z, Tian X, Zhu J, et al. Metformin suppresses UHMWPE particle-induced osteolysis in the mouse calvaria by promoting polarization of macrophages to an anti-inflammatory phenotype. *Mol Med*. 2018;24(1):20. doi:10.1186/s10020-018-0013-x
52. Kandahari AM, Yang X, Laroche KA, Dighe AS, Pan D, Cui Q. A review of UHMWPE wear-induced osteolysis: the role for early detection of the immune response. *Bone Res*. 2016;4(1):16014. doi:10.1038/boneres.2016.14
53. Hutchins AP, Diez D, Miranda-Saavedra D. The IL-10/STAT3-mediated anti-inflammatory response: recent developments and future challenges. *Briefings Func Genomics*. 2013;12(6):489–498. doi:10.1093/bfgp/elt028

54. Degboé Y, Rauwel B, Baron M, et al. Polarization of rheumatoid macrophages by TNF targeting through an IL-10/STAT3 mechanism. *Front Immunol*. 2019;10:3. doi:10.3389/fimmu.2019.00003
55. Nikaein N, Tuerxun K, Cedersund G, et al. Mathematical models disentangle the role of IL-10 feedbacks in human monocytes upon proinflammatory activation. *J Biol Chem*. 2023;299(10):105205. doi:10.1016/j.jbc.2023.105205
56. Gao XR, Ge J, Li WY, Zhou WC, Xu L, Geng DQ. NF-κB/let-7f-5p/IL-10 pathway involves in wear particle-induced osteolysis by inducing M1 macrophage polarization. *Cell Cycle*. 2018;17(17):2134–2145. doi:10.1080/15384101.2018.1515549
57. Zhang X, Edwards JP, Mosser DM. Dynamic and transient remodeling of the macrophage IL-10 promoter during transcription. *J Immunol*. 2006;177(2):1282–1288. doi:10.4049/jimmunol.177.2.1282
58. Carlini V, Noonan DM, Abdalalem E, et al. The multifaceted nature of IL-10: regulation, role in immunological homeostasis and its relevance to cancer, COVID-19 and post-COVID conditions. *Review*. 2023;14. doi:10.3389/fimmu.2023.1161067
59. Németh K, Leelahavanichkul A, Yuen PST, et al. Bone marrow stromal cells attenuate sepsis via prostaglandin E2–dependent reprogramming of host macrophages to increase their interleukin-10 production. *Nature Med*. 2008;15(1):42–49. doi:10.1038/nm.1905
60. Wang J, Xia J, Huang R, et al. Mesenchymal stem cell-derived extracellular vesicles alter disease outcomes via endorsement of macrophage polarization. *Stem Cell Res Therapy*. 2020;11(1):424. doi:10.1186/s13287-020-01937-8
61. Chen Y, Yang L, Li X. Advances in Mesenchymal stem cells regulating macrophage polarization and treatment of sepsis-induced liver injury. *Front Immunol*. 2023;14:1238972. doi:10.3389/fimmu.2023.1238972
62. Bao J, Wang Z, Yang Y, et al. Interleukin-17 alleviates erastin-induced alveolar bone loss by suppressing ferroptosis via interaction between NRF2 and p-STAT3. *J Clin Periodontol*. 2023;51(2):233–250. doi:10.1111/jcpe.13898
63. Abu-Amer W, Arra M, Clohisy JCF, Abu-Amer Y, Swarnkar G. Targeting vascular endothelial growth factor ameliorates PMMA-particles induced inflammatory osteolysis in murine calvaria. *Bone*. 2019;123:86–91. doi:10.1016/j.bone.2019.03.025
64. Moran MM, Li J, Shen Q, et al. Evidence of an allostatic response by intestinal tissues following induction of joint inflammation. 2025.
65. Yang M, Chen X, Hu X, et al. The NF-κB-SLC7A11 axis regulates ferroptosis sensitivity in inflammatory macrophages. *Cell Insight*. 2025;4(4):100257. doi:10.1016/j.cellin.2025.100257
66. Zhou X, Ye C, Jiang L, et al. The bone mesenchymal stem cell-derived exosomal miR-146a-5p promotes diabetic wound healing in mice via macrophage M1/M2 polarization. *Mol Cell Endocrinol*. 2024;579:112089. doi:10.1016/j.mce.2023.112089
67. Connors JP, Stelzer JW, Garvin PM, Wellington IJ, Solovyova O. The role of the innate immune system in wear debris-induced inflammatory peri-implant osteolysis in total joint arthroplasty. *Bioengineering*. 2022;9(12). doi:10.3390/bioengineering9120764
68. Ma T, Liu Q, Zhang Z, et al. Fused exosomal targeted therapy in periprosthetic osteolysis through regulation of bone metabolic homeostasis. *Bioactive Materials*. 2025;50:171–188. doi:10.1016/j.bioactmat.2025.04.006
69. Tang J, Wang X, Lin X, Wu C. Mesenchymal stem cell-derived extracellular vesicles: a regulator and carrier for targeting bone-related diseases. *Cell Death Discovery*. 2024;10(1):212. doi:10.1038/s41420-024-01973-w
70. Colao IL, Corteling R, Bracewell D, Wall I. Manufacturing Exosomes: a Promising Therapeutic Platform. *Trends Mol Med*. 2018;24(3):242–256. doi:10.1016/j.molmed.2018.01.006
71. Zhu X, Badawi M, Pomeroy S, et al. Comprehensive toxicity and immunogenicity studies reveal minimal effects in mice following sustained dosing of extracellular vesicles derived from HEK293T cells. *J Extracell Vesicles*. 2017;6(1):1324730. doi:10.1080/20013078.2017.1324730
72. Rani S, Ryan AE, Griffin MD, Ritter T. Mesenchymal stem cell-derived extracellular vesicles: toward cell-free therapeutic applications. *Mol Therap*. 2015;23(5):812–823. doi:10.1038/mt.2015.44
73. Lemmerman LR, Balch MHH, Moore JT, et al. Nanotransfection-based vasculogenic cell reprogramming drives functional recovery in a mouse model of ischemic stroke. *Science Advances*. 2021;7(12). doi:10.1126/sciadv.abd4735